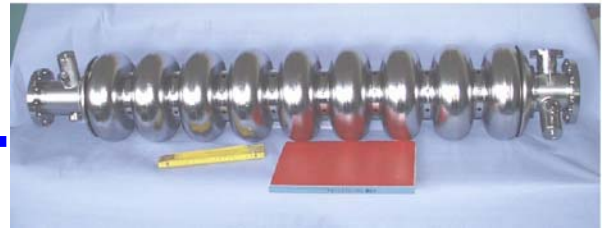




SRF



Report on Fast Piezo Blade Tuner (UMI Tuner) for SRF Resonators Design and Fabrication

C. Pagani, A. Bosotti, P. Michelato, R. Paparella, N. Panzeri, P. Pierini, F. Puricelli
INFN Sezione di Milano LASA, Italy

G. Corniani,
ZANON, Schio, Italy

Abstract

We report on this note the design of a fast tuning device for high gradient superconducting cavities for ILC. This device is an evolution of a coaxial tuner solution we developed for TTF superstructures and that performed as expected in terms of stiffness, frequency sensitivity and tuning capabilities both in CHECHIA and during TTF operations. Now, in order to compensate the Lorentz forces detuning foreseen at 35 MV/m, fast elements have been integrated in the tuner and the designed configuration is presented here.

Introduction

In the ILC project an accelerating field of 35 MV/m and a filling factor higher than that of the TTF are expected. Unfortunately such a high accelerating field requires a suitable solution in order to reduce the Lorentz forces detuning.

It has been proven that a piezoelectric tuner system will permit efficient cavity operation at the gradient of 35MV/m [1] but the design requirements are very tight due to the particular working conditions (cryogenic temperature) and to the need to increase the filling factor. For this reason we developed a coaxial tuner solution (blade tuner) inspired by the idea described in [2] and two prototypes were built and tested in CHECHIA horizontal cryostat and on the so called superstructure in 2002 [3]. During both tests the blade tuner performed as expected in terms of stiffness, frequency sensitivity and tuning capabilities.

Later on in order to compensate the Lorentz forces detuning foreseen at 35 MV/m, fast elements have been integrated in the blade tuner and the designed configuration is presented in this report. The compatibility of the proposed solution with the TESLA/ILC cavities has been proved by means of FE analysis while two complete systems are under fabrication for experimental tests. Its main characteristics are no additional longitudinal space required, usability with minor modification with every SC cavity and possible use of different piezoelectric or magnetostrictive actuators.

1. Design Requirements

In the designing of the tuning device it has to be considered that the static Lorentz force detuning strongly depends from the global stiffness of the cavity. As shown in [4], increasing the boundary stiffness will decrease the static Lorentz force detuning and increase the global stability and strength of the cavity. Moreover in [5] it is shown that a contingent interaction between the cavity natural frequencies and the RF repetition rate could lead to an increase of the Lorentz forces detuning effect. For these reasons the end dishes, helium tank and tuner system have to be as stiffer as possible, but such as to avoid that the structure eigenfrequencies be in the RF repetition rate frequency range.

In the case of the TESLA cavities the following parameters have been considered:

- bandwidth: 434 Hz
- cavity sensitivity to axial stretch: 404 kHz/mm

In order to fulfill the tunability requirements of the TESLA project and on the bases of currents warm-cold frequency reproducibility test at the TTF, the values reported in Table 1 have been taken into consideration as minimum frequency shifts that the tuner must be capable to impose to the cavity.

Table 1: Guidelines for a TESLA cavity tuner.

	Frequency range [kHz]	Axial movement [μm]
Slow tuning	~ 500	~ 1500
Fast tuning	~ 1	~ 3

The tuning system is made of the blade tuner, driven by a stepping motor which provides the slow tuning capabilities, and a fast part that provides the Lorentz forces compensation. In the present design the fast part can accommodate two piezos of different length (from 36 to 72 mm) but if necessary they can be substituted with magnetostrictive elements. The helium tank has been modified too: the new one is split in two halves joined by a bellow in order to allow the variation of the cavity length imposed by the coaxial tuner.

2. Mechanical Characterization of the UMI Tuner

The piezo blade tuner is mainly composed of three parts (Figure 1):

- The rings-blades assembly, that provides the slow tuning to the cavity. This is the main tuner mechanism and consists of a three-ring bending system. One of the external rings is rigidly connected to the helium tank (Figure 2), while the central one is divided in two halves. The rings are connected by welded thin titanium plates (blades) at an angle which transforms the azimuthal rotation (in opposite directions) of the two halves of the central ring into a variation of the distance between the end rings, producing elastic change of the cavity length.
- The leverage mechanism: the azimuthal rotation of the central rings is provided by a leverage system connected to a stepping motor. The leverage system amplifies the torque of the stepping motor, contemporarily increasing the tuning sensitivity. The maximum axial displacement foreseen for the blade tuner is $w = \pm 1.5$ mm.;
- The piezo actuator part, that, during operation, can provide the fast tuning capabilities needed for Lorentz force detuning compensation and microphonics stabilization.

These three parts will be analyzed and fully explained in the following sections, while the detailed mechanical drawings, showing the geometry of all the tuner parts are reported in the Appendix 2.

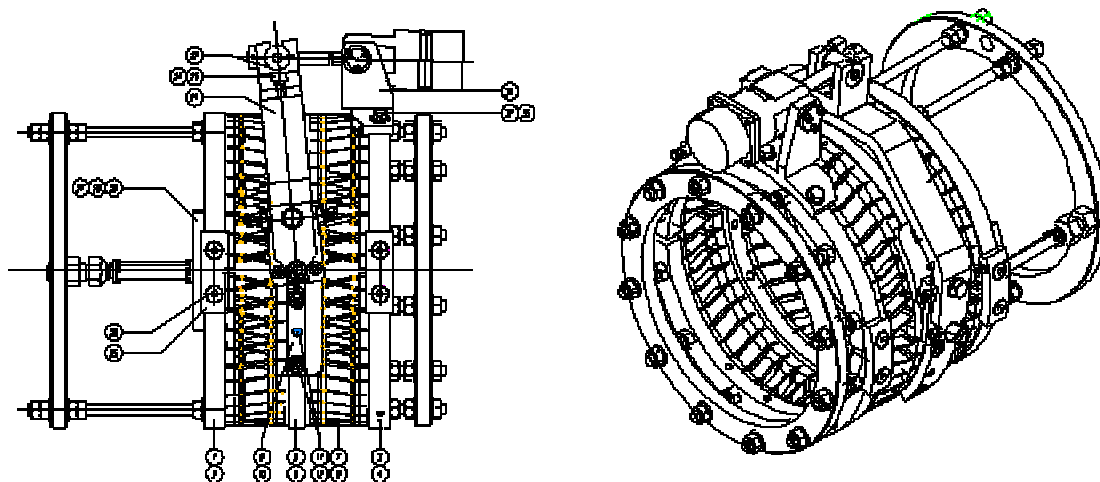


Figure 1: 3D drawings of the piezo blade tuner

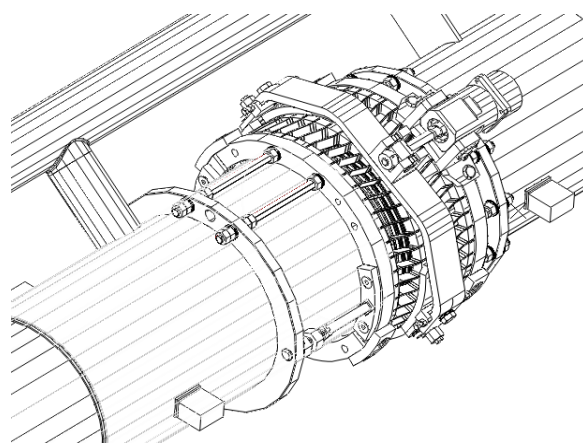


Figure 2: The tuner installed on the helium tank

2.1. Parameters used in mechanical calculation

The material characteristics used for the mechanical analyses are reported in Table 2.

Table 2: mechanical characteristics.

Parameter	Value	Units
Rings and blades material	Ti Gr2	-
Jaw with pin, operating bracket	Aisi 316L	-
Motor and bearing support	Aisi 316L	-
Connecting rod	Ot MS58	-
Titanium Grade 2 material		
Young Modulus, E_x	105	GPa
Density, ρ	4500	kg/m ³
Major Poisson ratio, ν_{xy}	0.37	-
Aisi 316L		
Young Modulus, E_x	191	GPa
Density, ρ	7850	kg/m ³
Major Poisson ratio, ν_{xy}	0.29	-
Ot MS58		
Young Modulus, E_x	105	GPa
Density, ρ	8400	kg/m ³
Major Poisson ratio, ν_{xy}	0.35	-

2.2. Mechanical characterization of leverage

2.2.1. Leverage kinematics

The ring-blade system has been designed with a parametrical model (in terms of the blade length and inclination) in order to define the structure kinematics and to provide the axial stiffness and tuning force compatibility. The working principle of the tuner is based on the deformation of the blades that deform from the rest position (slant of 15° with respect to the central axis) to a different configuration producing an elongation or a shortening of the tuner itself (see Figure 3).

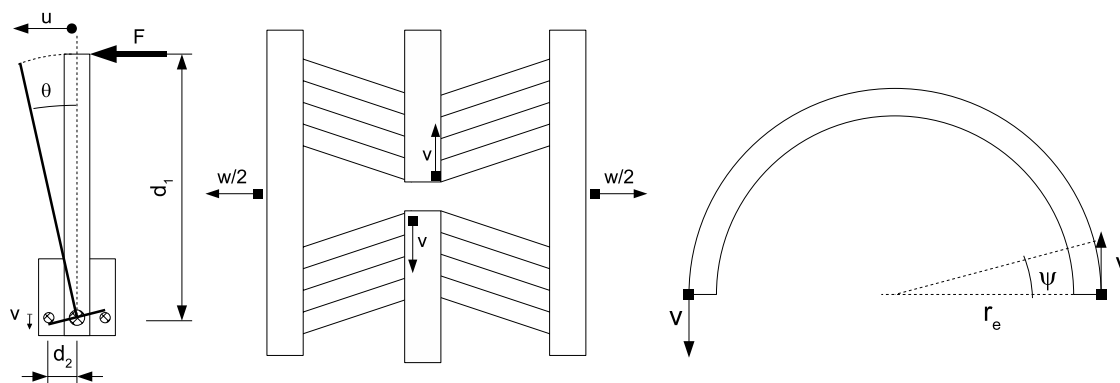


Figure 3: cinematic description of the fine tuning system

This deformation is generated by the rotation of the central rings with respect to the lateral ones. In order to reduce to nearly zero the relative rotation of the lateral rings and to balance the torsional moments, the central rings rotate in opposite directions and the blade are assembled symmetrically with respect to the horizontal plane. Let us compute the maximum displacement u that can be applied to the leverage mechanism.

From the technical drawings, (see Appendix 2), the following dimensions can be obtained:

$$\begin{aligned}d_1 &= 162.5 + 12 + 30 = 204.5 \text{ mm} \\d_2 &= 35/2 = 17.5 \text{ mm} \\r_e &= 300/2 = 150 \text{ mm}\end{aligned}\quad (2.1)$$

And, from simple geometrical considerations:

$$\begin{aligned}\theta &= \arctan \frac{u}{d_1} \\v &= d_2 \tan \theta = u \frac{d_2}{d_1} \\\psi &\cong \frac{v}{r_e} = \frac{u}{r_e} \frac{d_2}{d_1}\end{aligned}\quad (2.2)$$

The maximum displacement that can be applied can be limited both by the contact of the central rings themselves and by the maximum movement of the mechanism:

- **limit displacement by contact of the central rings**

Central ring distance is of 7 mm only, therefore, neglecting the mechanism deformations:

$$\begin{aligned}v_{\max} &= 7/2 = 3.5 \text{ mm} \Rightarrow \psi_{\max} = \frac{3.5}{150} = 0.023^r = 1.337^\circ \\u_{\max} &= 3.5 \frac{204.5}{17.5} = 40.9 \text{ mm}\end{aligned}\quad (2.3)$$

- **limit displacement by mechanism capabilities**

The critical part concerning the mechanism capabilities is the piece n. 13 of Figure 33 (connecting plate) which has two slots with eccentricity of 1.25 mm (see Figure 4).

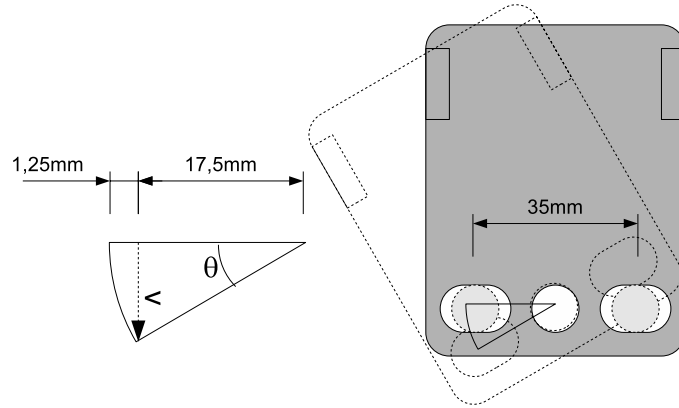


Figure 4: leverage-rings connecting plate

With simple geometric considerations and neglecting the mechanism deformations one obtains:

$$\begin{aligned}\theta_{\max} &= \arctan \frac{17.5}{18.75} = 21^\circ \Rightarrow v_{\max} = 18.25 \sin \theta_{\max} = 6.7 \text{ mm} \\u_{\max} &= d_1 \tan \theta_{\max} = \pm 82 \text{ mm}\end{aligned}\quad (2.4)$$

So the maximum displacement of the mechanism is presently limited by the contact of the two central rings: if a bigger range of tuning is desired, the geometry of the central rings can be simply modified by increasing the space between them.

2.2.2. Finite element model

Due to the complexity of the mechanism a simplified model has been used: some parts were neglected and, if possible, the connections have been considered as bonded. The boundary conditions are reported in Figure 5; while the finite element model is reported in Figure 6. It consists of 18547 elements and 36409 nodes.

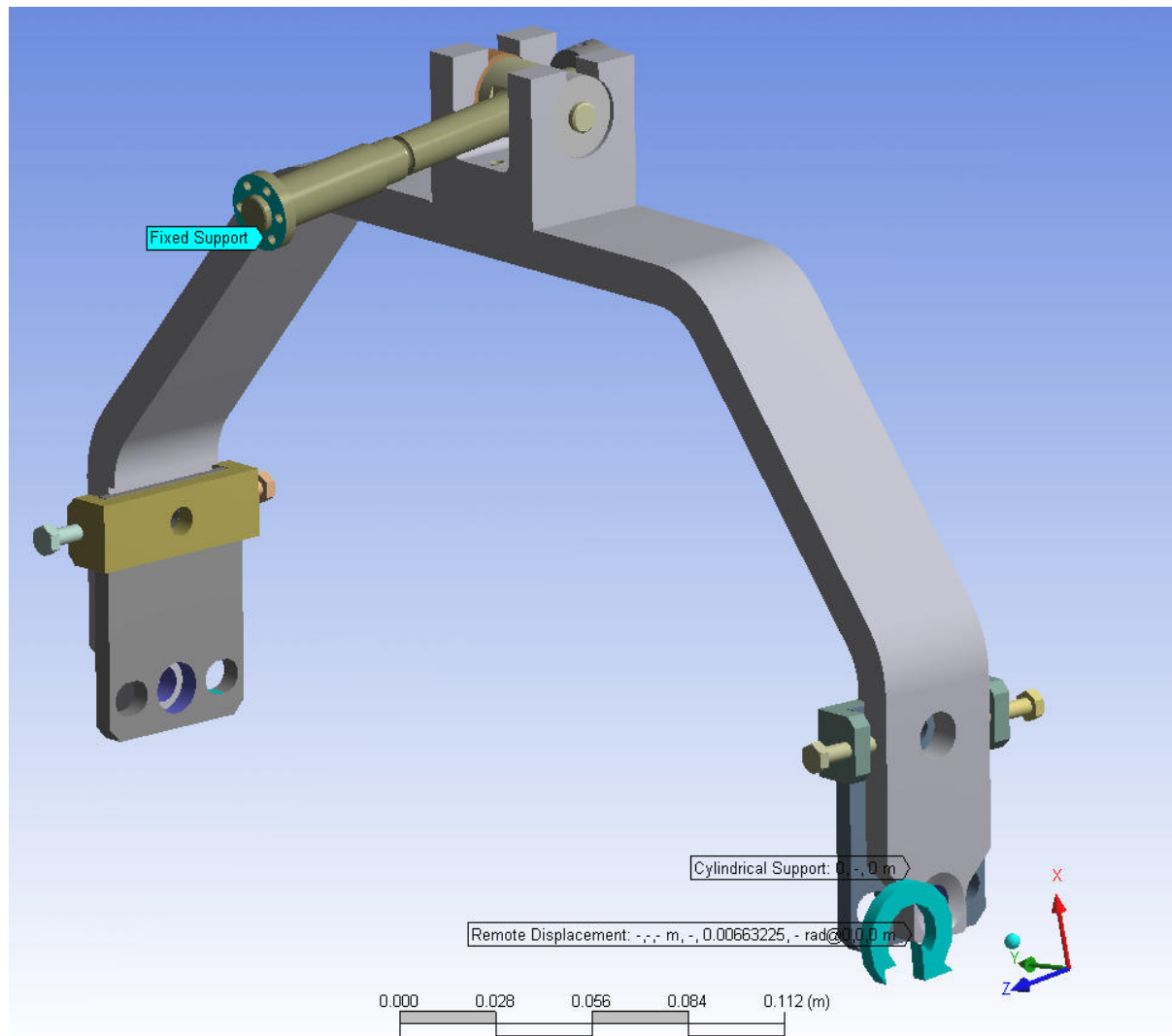


Figure 5: boundary conditions applied to the mechanism

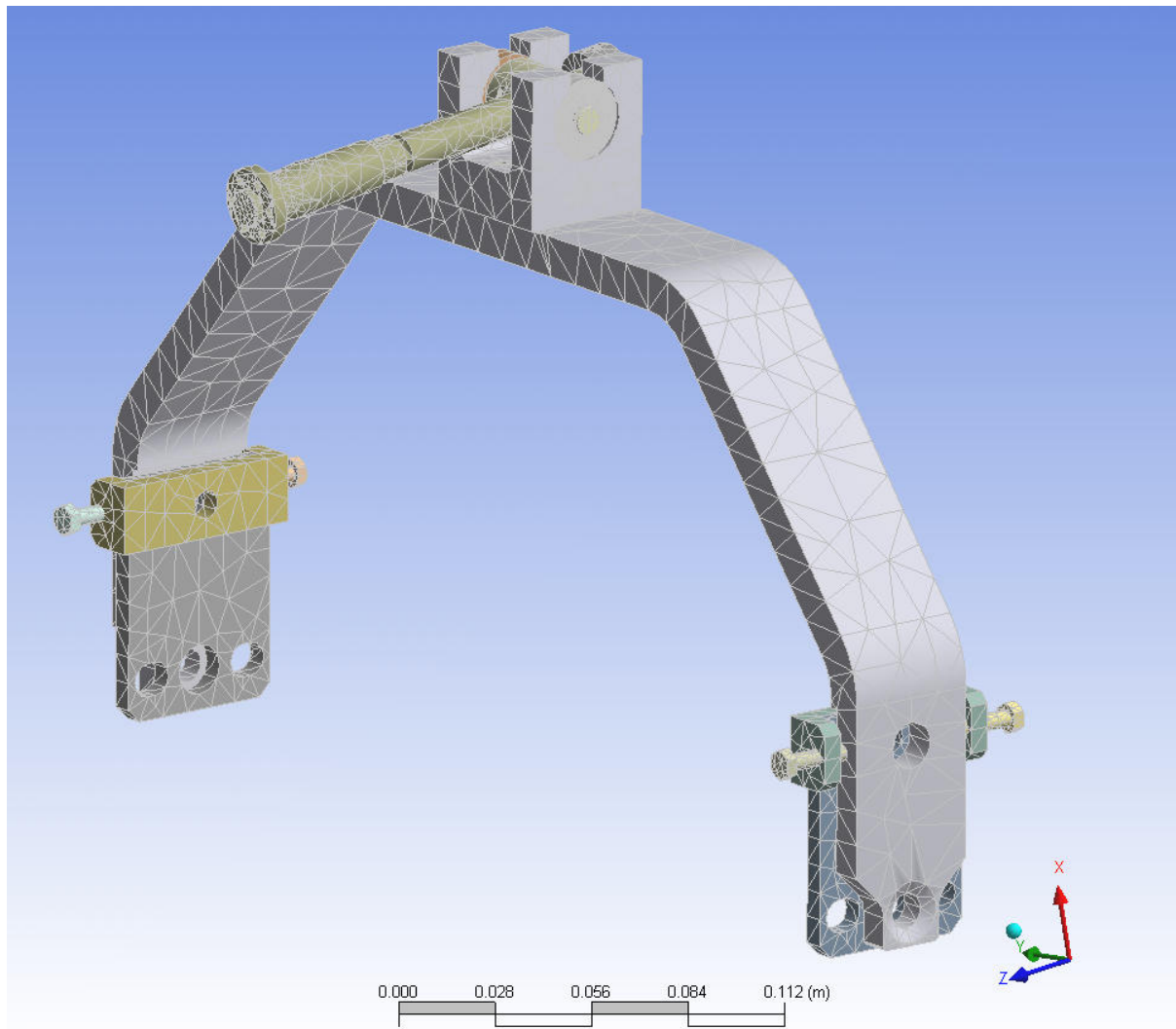


Figure 6: finite element model of the mechanism

2.2.3. Leverage analysis

A finite element analysis (FEA) of the leverage system has been performed in order to evaluate its stiffness and the maximum stresses. These results, together with the results of the same FEA of the rings-blades assembly, will be used to obtain the behavior of the whole tuner.

The analysis has been performed by imposing a rotation of 0.38° to the connecting rods, equivalent to a 0.0443° rotation of the central rings ($v = 0.116$ mm), while the driving shaft is fixed at its far end. A total reaction of 722 Nm at the location of the applied rotation has been found as result of the FEA.

The obtained displacements and stresses are reported in Figure 7 and Figure 8.

The leverage mechanism total stiffness is:

$$k_{mech} = \frac{722}{0.0443} = 16285 \text{ Nm/}^\circ = 933103 \text{ Nm} \quad (2.5)$$

where the rotation considered is the rotation of the central rings.

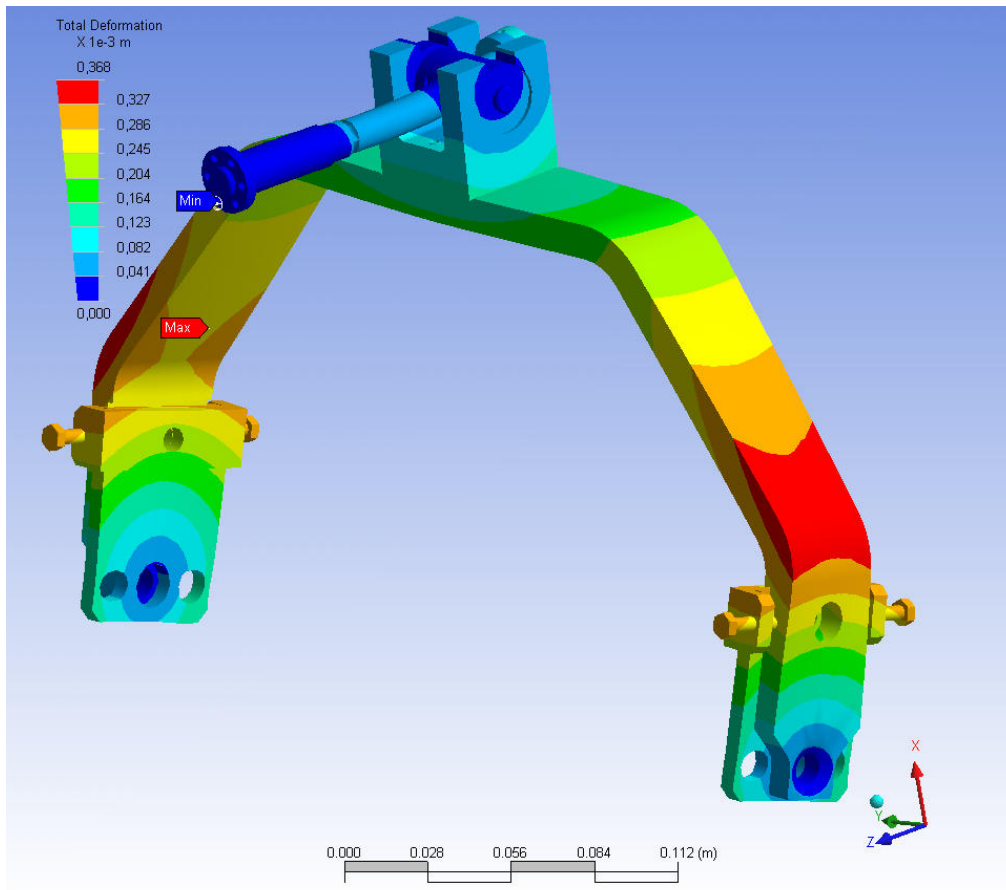


Figure 7: displacements of mechanism

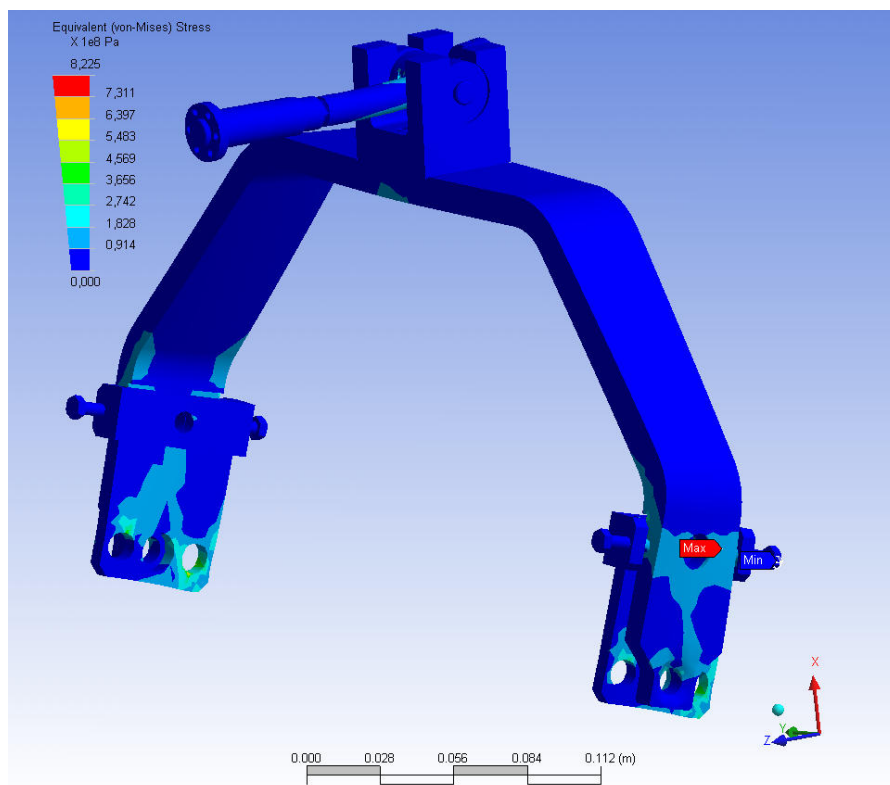


Figure 8: von Mises stresses of mechanism

2.3. Mechanical characterization of blade tuner

The blade tuner, used for the slow tuning of the cavity, is composed of two symmetric halves with respect to the horizontal plane. The two parts, that in the following will be called “half-tuner”, are made of three rings and two series of blades, positioned symmetrically with respect to the central ring (see technical drawing in Appendix 2). This configuration allows obtaining an axial movement of the lateral rings by means of an opposite rotation of the two central ones. Torsion and shear forces on the helium tank are also minimized.

2.3.1. Finite element model

Two different finite element models were considered: the first is a 2D model for the blade alone (see Figure 9) and the second is a 3D model for the half tuner (see Figure 10).

The blade model consists of 102 nodes and 101 beam elements, while the half tuner model consists of 143297 nodes, 71364 solid elements and 3864 shell elements.

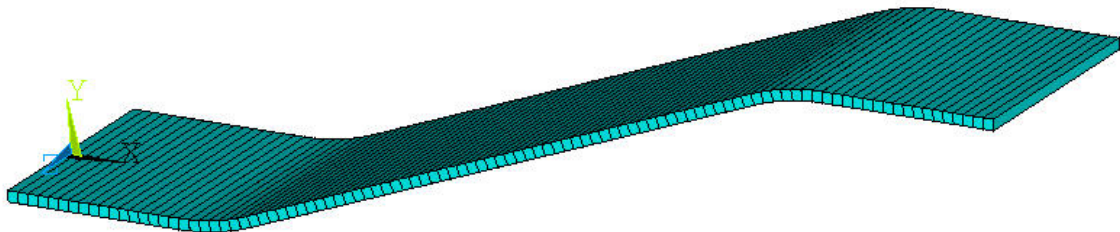


Figure 9: 2D finite element model of the blade (with blade width representation)

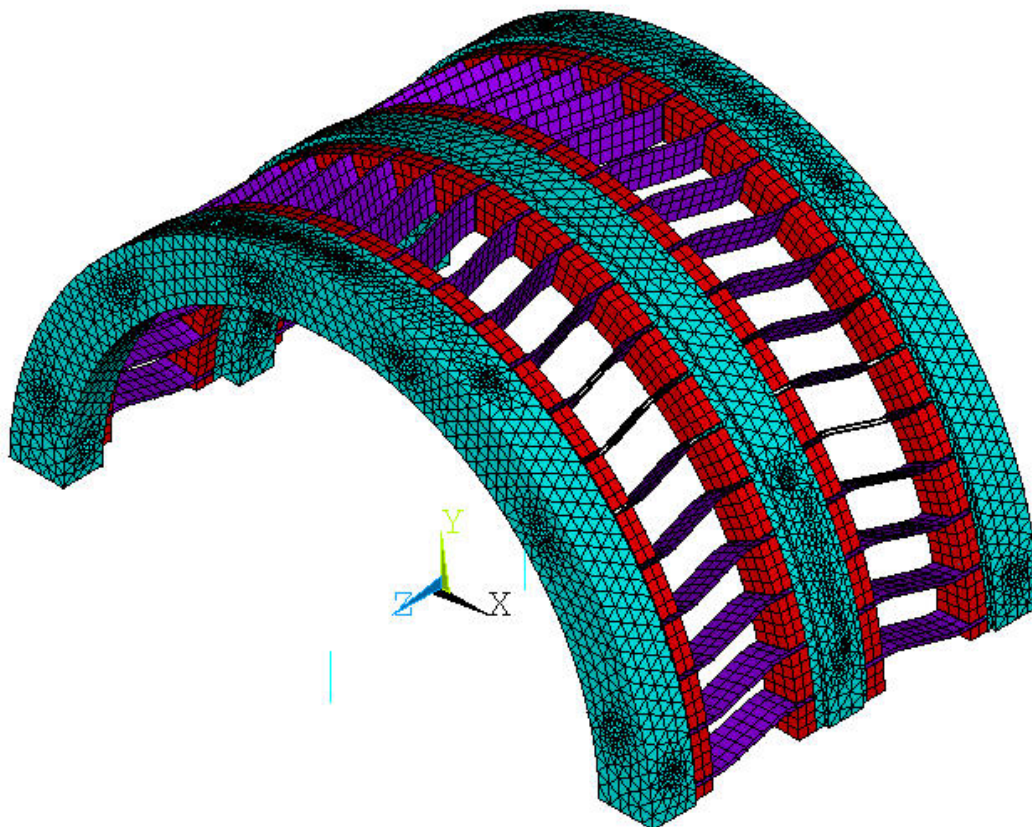


Figure 10: 3D finite element model of half tuner

2.3.2. Single blade analysis

The 2D model of the blade allows considering only the in-plane deformations. Nevertheless a useful and complete estimation of the tuner stiffness can be obtained by performing three analyses with different boundary. The three cases, shown in Figure 11, represent the possible behavior of the tuner when all symmetries have already been considered. The single blade FE analysis results are reported in Table 3.

Table 3: single blade analyses results

Load case	Δu [mm]	Δv [mm]	F_y [N]	M [Nmm]
1	-0.074965	0.31091	1	-20.462
2	-0.01808	0.074864	0	-3.9454
3	-0.0002971	0	0.2363	0.95920

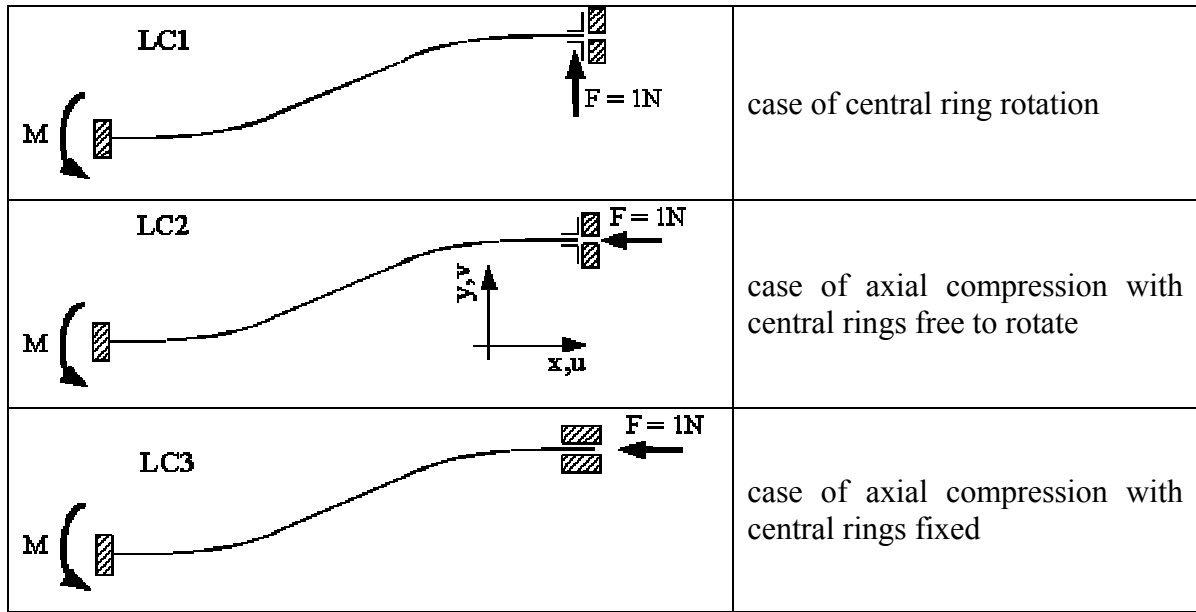


Figure 11: load cases considered for the analysis of the blade

Considering that $2 \times 2 \times 23 = 92$ blades are used for each half tuner the following compliance and stiffness are obtained, using the values reported in Table 3 and the geometrical dimensions reported in the mechanical drawings (see Appendix 2):

- load case 1: rotation of the central ring without constraints

$$C_{blade}^{mix} = \frac{\Delta u}{F \cdot r_b} = \frac{-0.074965}{1 \cdot 140.5} = -5.336 \cdot 10^{-4} \text{ [N}^{-1}\text{]} \quad (2.6)$$

$$C_{blade}^{rot} = \frac{\arcsin \frac{\Delta v}{r_b}}{F \cdot r_b} = \frac{\arcsin \frac{0.31091}{140.5}}{1 \cdot 140.5} = 1.575 \cdot 10^{-6} \text{ [N}^{-1}\text{mm}^{-1}\text{]} \quad (2.7)$$

$$C_{half-tuner}^{mix} = \frac{2}{92} C_{blade}^{mix} = -11.599 \cdot 10^{-6} \text{ [N}^{-1}\text{]} \quad (2.8)$$

$$C_{half-tuner}^{rot} = \frac{1}{92} C_{blade}^{rot} = 1.712 \cdot 10^{-8} \text{ [N}^{-1}\text{mm}^{-1}\text{]} \quad (2.9)$$

- load case 2: compression of the tuner with central ring free to rotate

$$C_{blade}^{mix} = \frac{\arcsin \frac{\Delta v}{r_b}}{F} = \frac{\arcsin \frac{0.074864}{140.5}}{1} = 5.328 \cdot 10^{-4} \text{ [N}^{-1}\text{]} \quad (2.10)$$

$$C_{blade}^{ax-free} = \frac{\Delta u}{F} = \frac{-0.01808}{-1} = 1.808 \cdot 10^{-2} \text{ [N}^{-1}\text{mm]} \quad (2.11)$$

$$C_{half-tuner}^{mix} = \frac{1}{46} C_{blade}^{mix} = 1.158 \cdot 10^{-5} \text{ [N}^{-1}\text{]} \quad (2.12)$$

$$C_{half-tuner}^{ax-free} = \frac{2}{46} C_{blade}^{ax-free} = 7.861 \cdot 10^{-4} \text{ [N}^{-1}\text{mm]} \quad (2.13)$$

- load case 3: compression of the tuner: the central ring cannot rotate

$$C_{blade}^{ax} = \frac{\Delta u}{F} = \frac{-0.0002971}{-1} = 2.971 \cdot 10^{-4} \text{ [N}^{-1}\text{mm]} \quad (2.14)$$

$$C_{half-tuner}^{ax} = \frac{2}{46} C_{blade}^{ax} = 1.292 \cdot 10^{-5} \text{ [N}^{-1}\text{mm]} \quad (2.15)$$

where:

r_b = mean radius of blades on tuner

C^{mix} = axial compliance due to a rotation of the central ring or vice versa

C^{rot} = torsional compliance due to a rotation of the central ring

$C^{ax-free}$ = axial compliance due to a axial displacement of the central ring when free to rotate

C^{ax} = axial compliance due to a axial displacement of the central ring

2.3.3. Half tuner analysis

The 3D analysis allows considering all possible boundary conditions. Keeping in mind the symmetries of the tuner, generalized displacements have been introduced to describe the relative movement of the central ring with respect to the lateral ones. These displacements (two translations and one rotation) are reported in Figure 12. The symbol u and w refer to the displacement in x and z directions, while ψ refers to the rotation around the z axis.

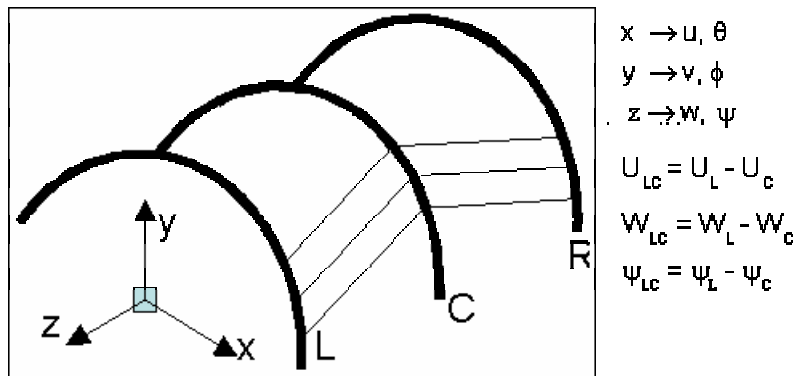


Figure 12: generalized displacements

Generalized forces are also introduced and associated to the respective relative displacement as explained in Figure 13.

By performing several analyses with only one generalized displacement active the following forces-displacements relations, relative to half tuner, have been obtained:

$$\begin{Bmatrix} \hat{F}_x \\ \hat{F}_z \\ \hat{M}_z \end{Bmatrix} = \begin{bmatrix} 14148 & 24950 & -840285 \\ 24950 & 164248 & -5449750 \\ -840285 & -5449750 & 184420000 \end{bmatrix} \begin{Bmatrix} u_{LC} \\ w_{LC} \\ \psi_{LC} \end{Bmatrix} \quad (2.16)$$

[N, Nmm] [mm, rad]

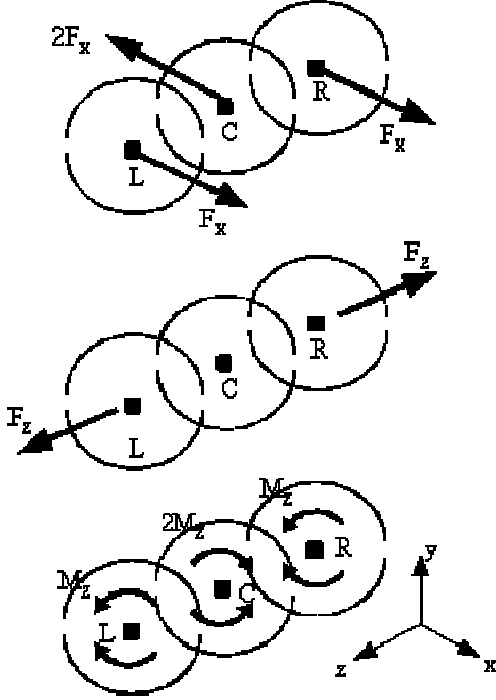


Figure 13: generalized forces

In these relations F_x , F_z and M_z are opposite to the reactions obtained by the finite element analyses and the symbol “^” is used when half tuner is considered. This matrix is the stiffness matrix of the half tuner when all symmetries are considered. The compliance matrix can be easily obtained, as reported in (2.17).

Combining the relations (2.16) and (2.17), one can write an equation set useful to compare the 3D FEA with the experimental results. For example using the (2.18) one can compare the simulation results with the compliance measured in the experimental case where the central ring is constrained by means of mechanical fixtures, so that it cannot rotate, but can move in the transversal direction, as we will see in section 2.3.5.

$$\begin{Bmatrix} u_{LC} \\ w_{LC} \\ \psi_{LC} \end{Bmatrix} = 10^{-6} \begin{bmatrix} 96.947 & -3.6144 & 0.33491 \\ -3.6144 & 312.266 & 9.2112 \\ 0.33491 & 9.2112 & 0.27914 \end{bmatrix} \begin{Bmatrix} \hat{F}_x \\ \hat{F}_z \\ \hat{M}_z \end{Bmatrix} \quad (2.17)$$

$$\begin{Bmatrix} u_{LC} \\ w_{LC} \\ \hat{M}_z \end{Bmatrix} = 10^{-6} \begin{bmatrix} 96.945 & -14.666 & 1.1998 \cdot 10^6 \\ -14.666 & 8.31622 & 32.99776 \cdot 10^6 \\ -1.1998 \cdot 10^6 & -32.99776 \cdot 10^6 & 3.58234 \cdot 10^{12} \end{bmatrix} \begin{Bmatrix} \hat{F}_x \\ \hat{F}_z \\ \psi_{LC} \end{Bmatrix} \quad (2.18)$$

2.3.4. Extensions of analyses to the whole tuner

The stiffness matrix of half tuner is here used to evaluate the behavior of the whole blade tuner (only the main tuner mechanism, without leverage and piezo actuator elements). The following assumptions are made:

- the degree of freedom in axial direction is considered between the two lateral rings;

- torsion, transversal force in x direction and associated displacements are relative to the central ring and are necessary in order to evaluate the behavior of the tuner equipped with the mechanism;
- $w_{LR}=w_L-w_R$
- $w_{LC}=w_{CR}=w_{LR}/2$
- $u_{LC}=-u_{CR}$
- $\psi_{LC}=-\psi_{CR}$

The only displacement variable that changes is w (the axial displacement) that now refers to the whole tuner, while the other displacements are always referred to half tuner (see Figure 13). In terms of forces, F_x and F_z are now applied to the whole tuner, while the torsion M_z is always applied to the half tuner. Therefore, considering the effects of the two half tuners and their double length, the following relations are obtained:

$$\begin{Bmatrix} u_{LC} \\ w_{LR} \\ \psi_{LC} \end{Bmatrix} = 10^{-6} \begin{bmatrix} +48.473 & -1.8072 & +0.3349 \\ -3.6144 & +312.27 & +18.422 \\ +0.1675 & +4.6056 & +0.2791 \end{bmatrix} \begin{Bmatrix} F_x \\ F_z \\ M_z \end{Bmatrix} \quad (2.19)$$

$$\begin{Bmatrix} F_x \\ F_z \\ M_z \end{Bmatrix} = \begin{bmatrix} 28296 & 24950.5 & -1680570 \\ 49901 & 164248 & -10899500 \\ -840285 & -2724875 & 184420000 \end{bmatrix} \begin{Bmatrix} u_{LC} \\ w_{LR} \\ \psi_{LC} \end{Bmatrix} \quad (2.20)$$

[N, Nmm] [mm, rad]

and combining relations (2.19) and (2.20) with the same philosophy of the half tuner case, one gets:

$$\begin{Bmatrix} u_{LC} \\ w_{LR} \\ M_z \end{Bmatrix} = 10^{-6} \begin{bmatrix} +48.473 & -7.333 & +1199.8 \cdot 10^3 \\ -14.666 & +8.3162 & +66995 \cdot 10^3 \\ +599.9 \cdot 10^3 & -16499 \cdot 10^3 & +3582340 \cdot 10^6 \end{bmatrix} \begin{Bmatrix} F_x \\ F_z \\ \psi_{LC} \end{Bmatrix} \quad (2.21)$$

2.3.5. Comparison with experimental tests

An experimental test has been performed on a blade tuner [3]. A prototype of the bending system has been fixed on a accurate measuring machine while the central ring was rigidly fixed by means of two proper mechanical fixtures to avoid internal rotation (in this configuration, due to the symmetry of the inner ring, the tuner is in the same configuration of the operative one, simulating a leverage system with infinite stiffening). The same measurements have been repeated with the leverage mechanism to check its influence too. The structure has been compressed along the axes with different loads while monitoring, with micrometric precision sensors (LVDT), the deformation of the mechanism. Pictures of the experimental setup are reported in Figure 14. The 3D finite element model allows simulating only the first configuration, that is, the tuner rigidly fixed with mechanical fixture. In Table 4 the compliances measured testing the two different configurations are reported together with the finite element analysis of the free central ring case and the two other following boundary condition cases, i.e.:

- when the central ring can move in x direction and the rotation in azimuthal direction is blocked by a mechanical fixture:
 - $F_x = 0$; $\psi_{LC} = 0$
- when the central ring cannot move in x direction:
 - $u_{LC} = 0$; $\psi_{LC} = 0$

The simplified 2D (single blade) analysis in the load cases #2 and #3 are also presented in Table 4 for sake of completeness. The compliance values reported in relations 2.13 and 2.15 are halved to extend the analysis to the whole tuner case.

Using the relations (2.21) with $F_x = 0$; $\psi_{LC} = 0$, one gets $w_{LR} = 8.3162 \cdot 10^{-6} \cdot F_z$, where a good agreement is found between the measured compliance of 12 $\mu\text{m/kN}$ and the one computed with FEA, 8.3162 $\mu\text{m/kN}$. The case when the constrain is the leverage mechanism is too difficult to model, so the comparison between theory and practice in the second boundary condition case has not been done.

Table 4: tuner axial compliances for different boundary conditions ($\mu\text{m/kN}$)

Boundary conditions	Experimental	2D model	3D model
Central ring cannot rotate, but can translate in axial direction	12	---	8.316
Central ring cannot rotate and translate	---	6.45	6.089
Central ring constrained by mechanism	40	---	--- ¹
Central ring free	---	393	312



Figure 14: pictures of experimental compression tests on blade tuner, showing both the experimental configurations.

¹ the 3D modeling of the constraining mechanism was not developed

2.3.6. Integration of fast elements

The detailed information obtained by the finite element analysis of the blade tuner, which provided accurate information, such as stresses, deformations and stiffness, has then been used for the integration of a fast tuning action based on piezoelectric actuators, which are subject to several requirements limiting the choice of possible design configurations.

First of all, the piezoelectric actuators (piezos) cannot be subject to tension forces, and bending and shear actions need to be carefully avoided. Moreover, in order to maximize their lifetime, a correct preload range needs to be guaranteed under all operating condition. In addition to that, the characteristic behavior of piezo operation at cryogenic temperatures, in terms of stroke and preload effects, is still a subject undergoing a systematic investigation, especially within the CARE program [6]. From all the considerations expressed above, and using as guidelines the typical values of the TESLA type structures in terms of cavity elasticity and tuning requirements (see Table 1), we have integrated the piezoelectric elements in the tuner design, by inserting two elements between one of the end rings and the corresponding flange on the He vessel, as shown in Figure 15.

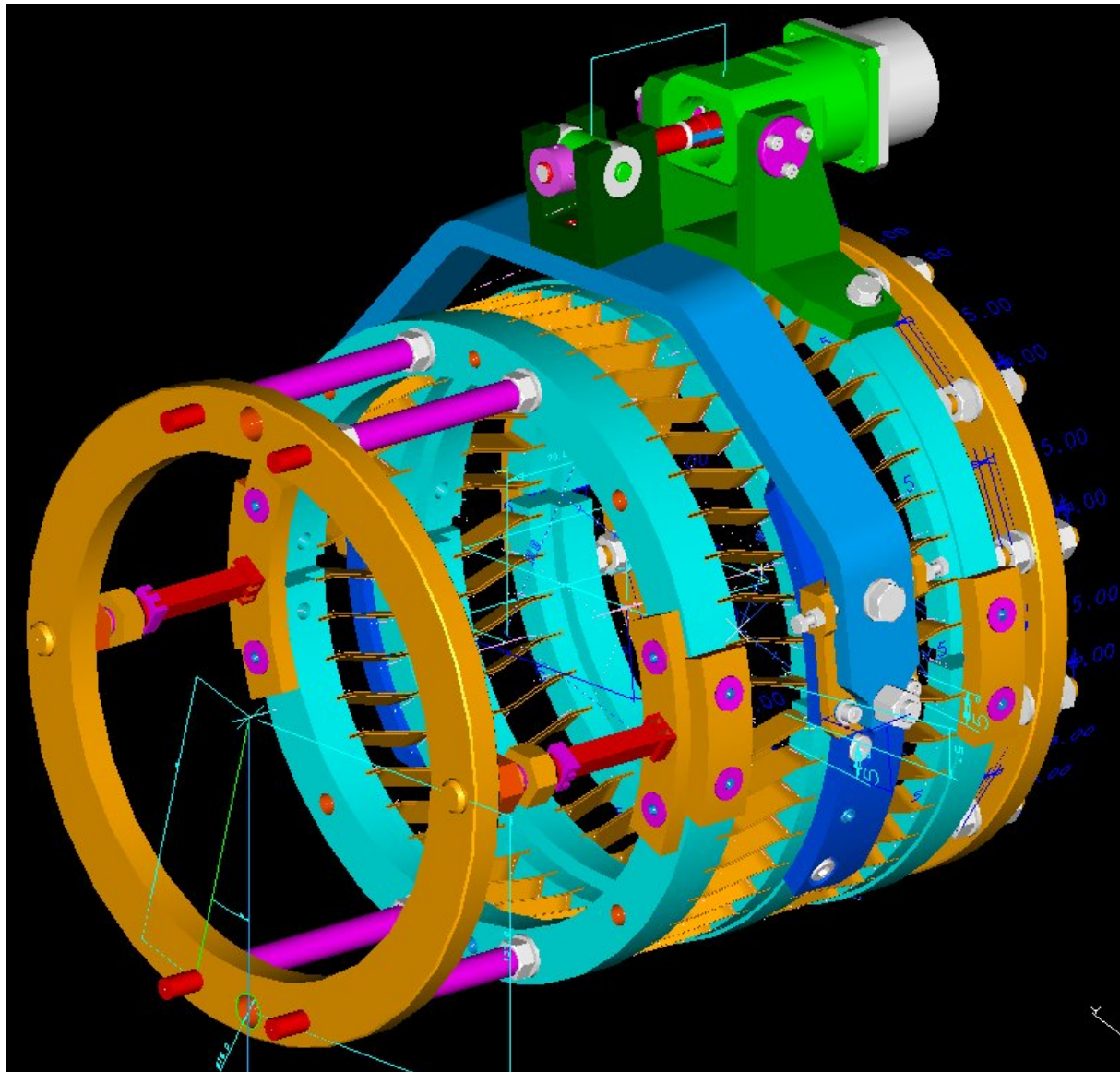


Figure 15: the piezo assisted tuner

The position of the piezo actuators has been carefully chosen in order to avoid possible stresses due to the deflection and vibration of the helium tank. Moreover four bars have been introduced in the design: they can be used both for transportation and safety means in case of piezo breakdown.

The active elements are kept in position by means of supports as shown in Figure 16: they can accommodate elements of length up to 72 mm and a spherical head is used in order to minimize shear and bending forces.

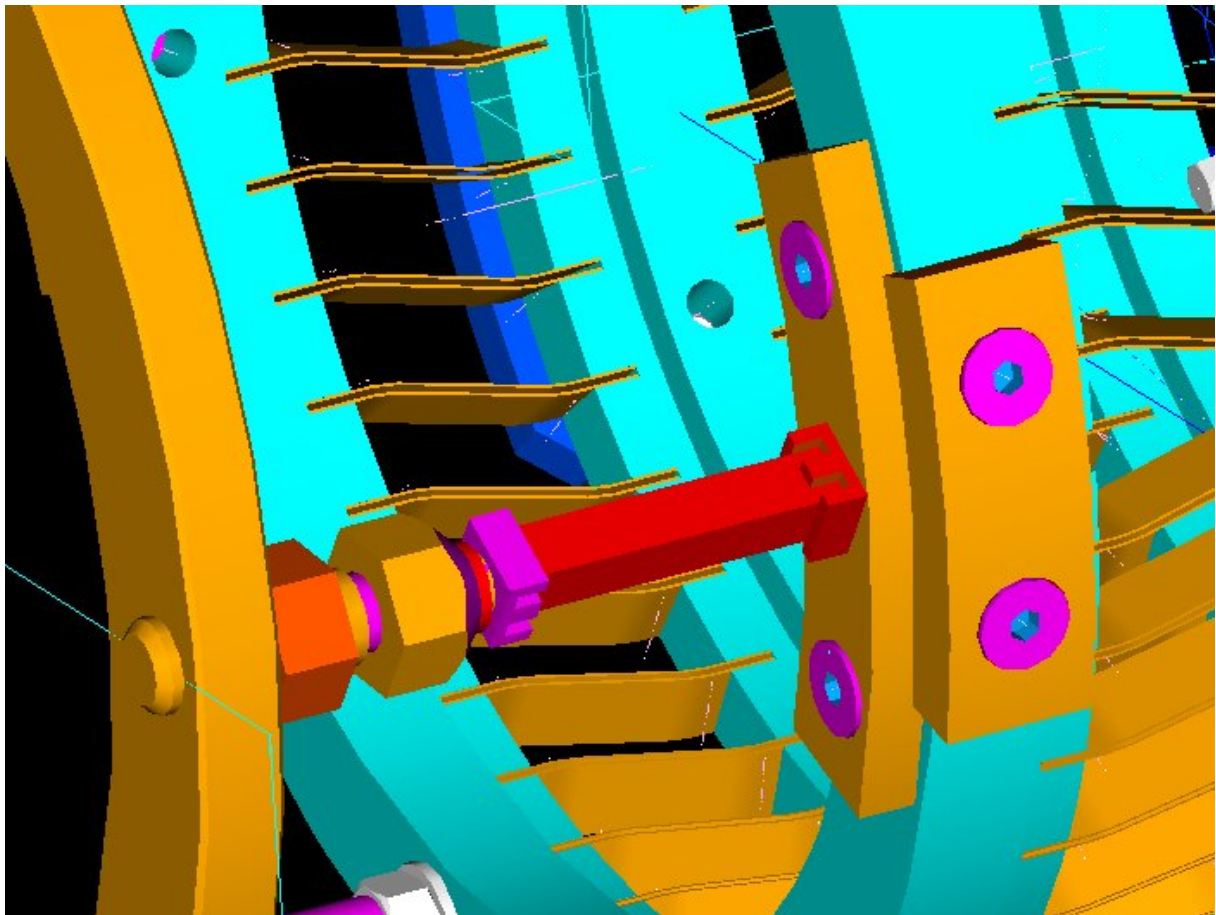


Figure 16: supports for the fixing of fast elements

3. Cavity Equipped With Helium Tank and Fast Tuner

The behavior of the cavity when equipped with helium tank and tuning system strongly depends from their stiffness. In this section axial and bending models are developed and commented out in order to evaluate the requirements for the piezo elements and check the compatibility with the technical specifications.

3.1. Mechanical characteristics

The mechanical characteristics of all parts at room temperature are here reported. The axial mechanical behavior of the full system (cavity + He tank + tuner) has been investigated parametrically by means of the spring model shown in Figure 17. The stiffness of every part,

for the TESLA cavity case, is reported in table 5, together with the material types, the elastic properties (Young module) and the legend of symbols used in Figure 17. The stiffness values were either derived from FEM analysis or measured experimentally [3].

Table 5: mechanical characteristics of all parts

Part	Material	Axial stiffness	C [$\mu\text{m}/\text{kN}$]	k [$\text{N}/\mu\text{m}$]	Notes
Helium tank	Ti Gr2	K_H	3.30	302.4	
Blade tuner	Ti Gr2	K_T	40.0	25	From exp.
Cavity	Nb	K_C	330.8	3.023	
Washer disk	NbTi	K_W	71.4	14.001	Both disks
Piezo actuator	PIC 255	K_P	4.76	2×10^5	
Tuner bellow	Ti Gr1	K_B	5263	0.19	

3.2. Axial analysis

In this section the axial model is presented and displacements and forces computed both for fine and fast tuning phases are shown.

3.2.1. Slow tuning

In the slow tuning phase the stepping motor applies a proper deformation to the blades in order to tune the cavity to the nominal frequency. Let us suppose that the blade tuner increases its nominal length of a quantity δ_t ; with this assumption the cavity will be stretched and the helium tank compressed. Globally the system remains in equilibrium. The scheme in Figure 17 shows the axial stiffness model where K_{WH} , K_P , K_B and K_C are the stiffness of end dishes plus the helium tank, piezo actuators, bellow and cavity.

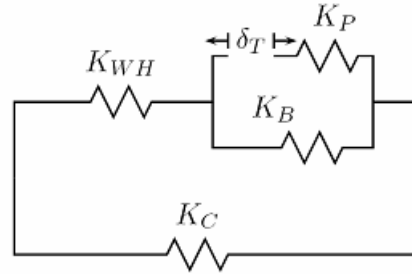


Figure 17: fine tuning axial model

From simple considerations the expression (3.1) for the global stiffness of end dishes and helium tank K_{WH} can be found:

$$K_{WH} = \frac{K_w K_H}{K_w + K_H} = 13.38 \text{ N}/\mu\text{m} \quad (3.1)$$

From equilibrium and congruence we can write the relation (3.2):

$$\left\{ \begin{array}{l} \delta_C = \delta_T + \delta_{WH} + \delta_P \\ \delta_B = \delta_T + \delta_P \\ F_C = K_C \delta_C \\ F_{WH} = K_{WH} \delta_{WH} \\ F_P = K_P \delta_P \\ F_B = K_B \delta_B \\ F_{WH} = -F_C \\ F_{WH} = F_B + F_P \end{array} \right. \quad (3.2)$$

Solving the consistent equations (3.2) it is possible to know the displacements of any part as a function of the tuner displacement:

$$\left\{ \begin{array}{l} \Delta = K_P K_{WH} + K_B (K_C + K_{WH}) + K_C (K_P + K_{WH}) \\ F_P = -\frac{K_P [K_C K_{WH} + K_B (K_C + K_{WH})]}{\Delta} \delta_T \\ F_B = \frac{K_P K_B (K_C + K_{WH})}{\Delta} \delta_T \\ F_{WH} = -\frac{K_P K_C K_{WH}}{\Delta} \delta_T \\ F_C = \frac{K_P K_C K_{WH}}{\Delta} \delta_T \\ \delta_P = -\frac{K_C K_{WH} + K_B (K_C + K_{WH})}{\Delta} \delta_T \\ \delta_B = \frac{K_P (K_C + K_{WH})}{\Delta} \delta_T \\ \delta_{WH} = -\frac{K_P K_C}{\Delta} \delta_T \\ \delta_C = \frac{K_P K_{WH}}{\Delta} \delta_T \end{array} \right. \quad (3.3)$$

The axial forces that every part has to withstand for a tuner displacement of 1 μm are reported in Table 6, while the displacements are reported in Table 7. As a result, 80% of the change of tuner length is transformed in a variation of the cavity length during the slow tuning action.

Table 6: axial forces for a tuner displacement of 1 μm . Tensile forces are positive

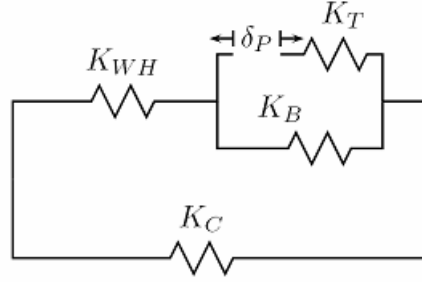
Part	Force for a $\delta_t = 1 \mu\text{m}$ [N]
Helium tank / End dishes	-2.4351
Blade tuner	-2.6227
Cavity	2.4351
Piezo actuators (total force)	-2.6227
Tuner bellow	0.1876

Table 7: Axial displacements for a tuner elongation of 1 μm . Elongations are positive

Part	Displacement for a $\delta_t = 1 \mu\text{m}$ [μm]
Helium tank / End dishes	-0.1820
Blade tuner	1
Cavity	0.8055
Piezo actuators	-0.0125
Tuner bellow	0.9875

3.2.2. Fast tuning

In the fast tuning phase the piezoelectric actuators perform length variations of the order of a few microns to compensate for the Lorentz force detuning, at each RF pulse. Let us suppose that the piezo actuators is subject to a length increase δ_p : with this assumption the cavity will be stretched and the helium tank compressed. Moreover the dynamic effects are not taken in account. Globally the system remains in equilibrium. The scheme in Figure 18 shows the axial stiffness model where K_{WH} , K_P , K_B and K_C are the stiffness of end dishes plus the helium tank, piezo actuators, bellow and cavity.

**Figure 18: fast tuning axial model**

From equilibrium and congruence:

$$\left\{ \begin{array}{l} \delta_C = \delta_T + \delta_{WH} + \delta_P \\ \delta_B = \delta_T + \delta_P \\ F_C = K_C \delta_C \\ F_{WH} = K_{WH} \delta_{WH} \\ F_T = K_T \delta_T \\ F_B = K_B \delta_B \\ F_{WH} = -F_C \\ F_{WH} = F_B + F_T \end{array} \right. \quad (3.4)$$

Solving the consistent equation it is possible to know the displacements of any part as a function of the piezo actuators displacement:

$$\left\{ \begin{array}{l}
 \Delta = K_T K_{WH} + K_B (K_C + K_{WH}) + K_C (K_T + K_{WH}) \\
 F_T = - \frac{K_T [K_C K_{WH} + K_B (K_C + K_{WH})]}{\Delta} \delta_P \\
 F_B = \frac{K_T K_B (K_C + K_{WH})}{\Delta} \delta_P \\
 F_{WH} = - \frac{K_T K_C K_{WH}}{\Delta} \delta_P \\
 F_C = \frac{K_T K_C K_{WH}}{\Delta} \delta_P \\
 \delta_P = - \frac{K_C K_{WH} + K_B (K_C + K_{WH})}{\Delta} \delta_P \\
 \delta_B = \frac{K_T (K_C + K_{WH})}{\Delta} \delta_P \\
 \delta_{WH} = - \frac{K_T K_C}{\Delta} \delta_P \\
 \delta_C = \frac{K_T K_{WH}}{\Delta} \delta_P
 \end{array} \right. \quad (3.5)$$

The axial forces that every part has to withstand for a piezo displacement of 1 μm are reported in Table 8, while the displacements are reported in Table 9.

Table 8: axial forces for a piezo actuators displacement of 1 μm . Tensile forces are positive

Part	Force for a $\delta_t = 1 \mu\text{m}$ [N]
Helium tank / End dishes	-2.2291
Blade tuner	-2.4009
Cavity	2.2291
Piezo actuators (total force)	-2.4009
Tuner bellow	0.1717

Table 9: axial displacements for a piezo actuators displacement of 1 μm . Elongations are positive

Part	Force for a $\delta_p = 1 \mu\text{m}$ [N]
Helium tank / End dishes	-0.1666
Blade tuner	-0.0960
Cavity	0.7374
Piezo actuators	1
Tuner bellow	0.9040

We note here that due to the low stiffness of the end dishes (particularly due to the weld lips), only 80 % of the displacement applied by the tuner is transferred to the cavity. For the fast tuning action a further contribution comes from the tuner stiffness, and only 74 % of the displacement applied by the piezos is transferred to the cavity. In particular, to provide the values reported in Table 1, the piezos have to assure a stroke greater than 4 μm at 2 K. The use of stiffer dishes or welding lips for the He tank connection would possibly reduce the requirements on tuner/piezo excursion.

It is also important to point out that the piezo preload is varying with the slow tuning action, therefore a suitable pre-tuning strategy needs to be assessed to ensure that during the slow tuning phase the preload remains within valid operation limits. Furthermore, we have to be sure that the piezo dynamic load is always lower than its blocking force (the force above which the piezo do not provide stroke). For the prototype case of two piezos, with a cross section of 10 x 10 mm, a blocking force of 4 kN (each) is expected therefore if we assume a load limit of 8 kN (obtained subtracting the 4 kN blocking force from the 12 kN nominal load limit) a maximum slow tuning action of ~ 1600 kHz can be safely applied, which is at least a factor of four higher than the current warm-cold frequency reproducibility at the TTF. For sake of safety a lower preload value is preferable. The experimental tests planned in the context of the CARE program to assess the thermal expansion of different piezo-ceramic materials together with the cold tests of the tuner prototypes, will further reduce the overall uncertainty of the preload at the tuner working point. Moreover, the needed cold tuning action is expected to further reduce for the case of a big industrial cavity production, like the one needed by the XFEL or ILC cases. Two NOLIAC SCMA/S1/A/10/10/40/200/60/4000 piezos will be used in the first two UMI tuner prototype tests. The main characteristics of this device are reported in APPENDIX 1. Physic Instrumente P-888.90 device characteristics are reported too, being this device a possible alternative to the former one. A picture of the two piezoceramics can be found in Figure 19.

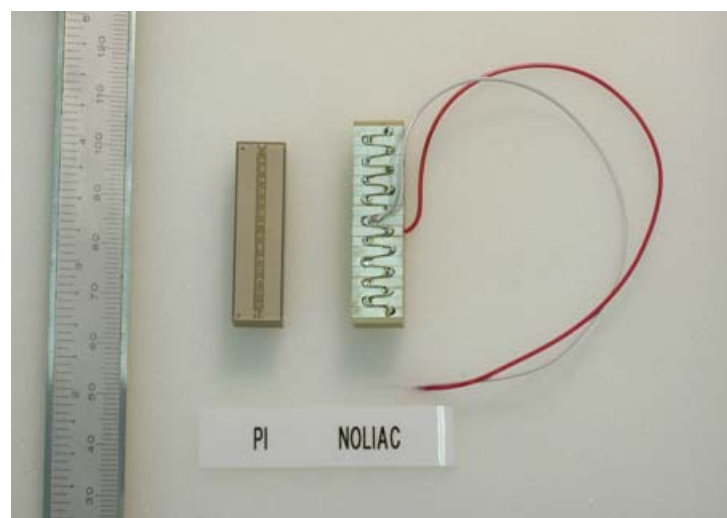


Figure 19: The PI P-888.90 and Noliac SCMA/S1..../60/4000 piezos.

4. Compatibility

Compatibility of the coaxial fast tuner with the TTF design has been checked in terms of transverse displacements (due to the gravity load) and mechanical eigenmodes.

4.1. Bending analysis

A bending analysis has been performed in order to check the vertical displacements of the cavity subject to its weight and to the weight of the tuner. This analysis is necessary because of the modification introduced in the helium tank design, now split in two halves joined by a bellow. To check the vertical displacements of the cavity and the stresses on the bellow, axisymmetric analyses with non axisymmetric load have been performed.

4.1.1. Cavity alone

This analysis is performed only for sake of comparison since the cavity remains alone only during the manufacturing phase. The model used consists of 1144 shell elements, 240 planar elements and 1445 nodes (see Figure 20). The cavity is supported by the end dishes.

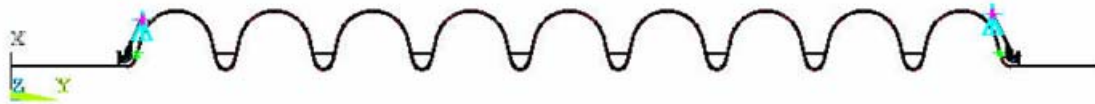


Figure 20: axisymmetric model for the cavity alone

The total dead load is of 230.4 N and the maximum deflection calculated is equal to 0.15 mm (see Figure 21)



Figure 21: vertical displacement of the cavity alone (magnification factor = 200)

4.1.2. Cavity equipped with helium tank

This case represents the cavity before being equipped with the piezo blade tuner. The model used consists of 1713 shell elements, 539 planar elements and 2369 nodes (see Figure 22). We point out that, in order to reduce the displacements, the pads that support the helium tank, at the coupler side (on the right in Figure 22) have been shifted by 150 mm towards the tuner position.

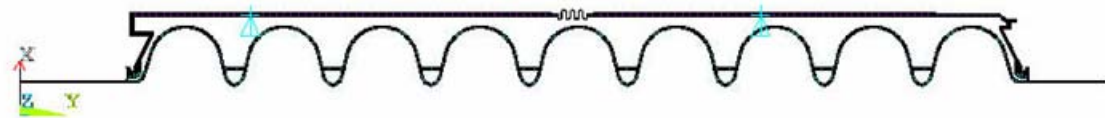


Figure 22: axisymmetric model for the cavity equipped with the helium tank

The total dead load is of 397.7 N and the maximum vertical displacement of the cavity is equal to 0.12 mm (see Figure 23). The most important displacements are reported in Table 10

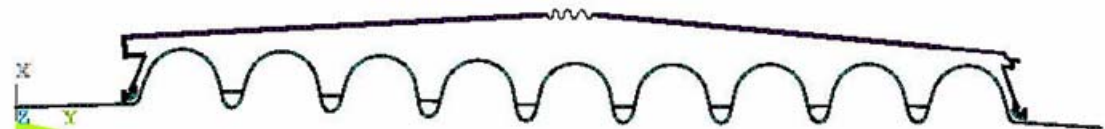


Figure 23: vertical displacement of the cavity and helium tank (magnification factor = 200)

Table 10: vertical displacements at the most important positions for cavity and helium tank

Position	Helium tank displ. [mm]	Cavity displ. [mm]
Left end	-0.036	-0.056
Center	+0.100	-0.120
Right end	-0.136	-0.177
Maximum deflection	-0.127	-0.259

```

ELEMENT SOLUTION
STEP=1
SUB =1
TIME=1
STR_VH {NORVG}
TOP
MAX =.120E-03
MIN =90035
SMX =.862E+07
    
```

ANSYS
 JUL 29 2005
 16:31:53

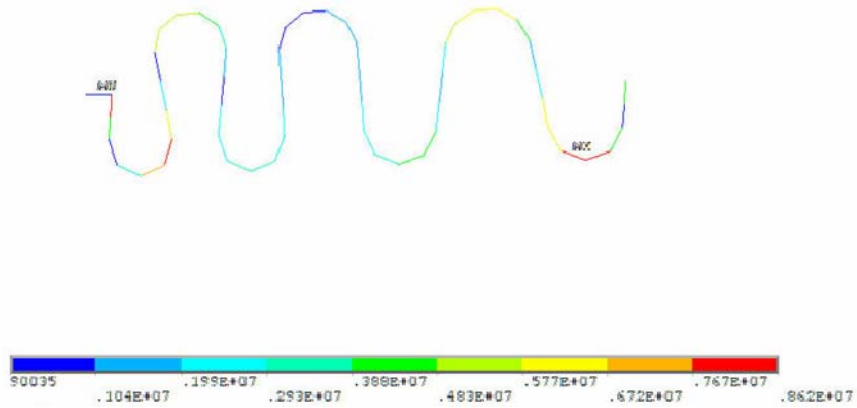


Figure 24: stresses in the bellow due to the dead loads

Neglecting the stress concentrations near the welding point, that are not accurately meshed, the maximum stress in the bellow is equal to 8.6 MPa, lower than the admissible stress (see Figure 24).

4.1.3. Cavity equipped with helium tank and piezo blade tuner

An axisymmetric model with non axisymmetric load has been implemented: it consists of 1713 2-nodes shell elements, 539 4-nodes planar elements and a total of 2369 nodes (see Figure 25); it accounts for the gravity load and neglects any vibration or external perturbation. In this configuration the tuner is considered only as a load and the stiffener effects due to the four safety bars are not considered.

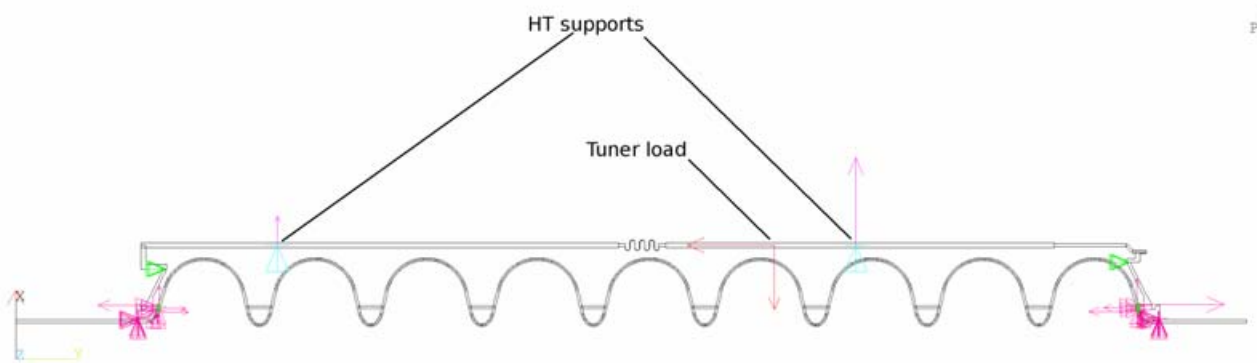


Figure 25: axisymmetric model for the analysis of vertical displacements

The total weight (cavity plus helium tank and piezo blade tuner) is of 598 N and the maximum vertical displacement of the cavity is of 0.144 mm in the up direction at the right end. Because the central lowering is of 0.115 mm (see Figure 26) the maximum sagging of the cavity respect to its ends is of $0.115 + 0.144 = 0.259$ mm, smaller than the specifications required for the fabrication tolerances of the cells (0.6 mm). The most important displacements are reported in Table 11.

```

1 NODAL SOLUTION
STEP=1
SUB =1
TIME=1
UX (AVG)
SYS=0
DXX =.119E-03
DYY =-.119E-03
DZZ =.645E-04
    
```

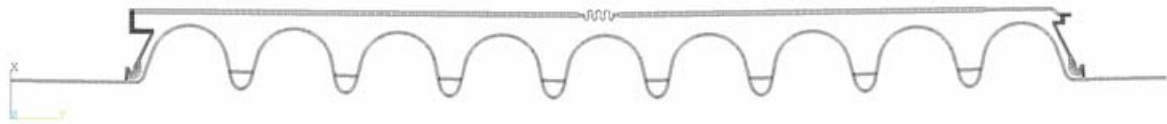


Figure 26: vertical displacements due to the dead loads

Table 11: vertical displacements at the most important positions

Position	Helium tank displ. [mm]	Cavity displ. [mm]
Left end	+0.027	+0.063
Center	-0.074	-0.115
Right end	+0.100	+0.144
Maximum deflection	-0.127	-0.259

Neglecting the stress concentrations near the welding point, that are not accurately meshed, the maximum stress in the bellow is equal to 6.3 MPa, lower than the admissible stress (see Figure 27).

```

ELEMENT SOLUTION
STEP=1
SUB =1
TIME=1
STR_VM2 (NOAVG)
TOP
DXX =.145E-03
DYY =-.418E+07
DZZ =.626E+07
    
```

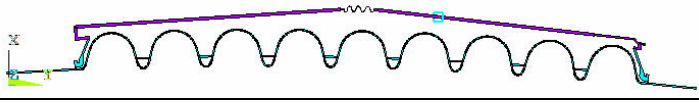
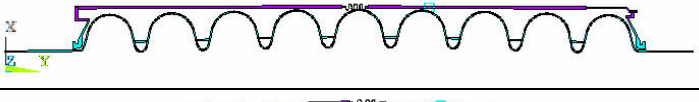




Figure 27: stresses in the bellow due to the dead loads and tuner weight

4.2. Eigenfrequency analysis

As seen in the design requirements, it is important to check that the first structure eigenfrequencies do not coincide with the frequency of RF repetition rate (1÷10 Hz) (or a multiple of it). This is verified as shown in Table 12.

Table 12: eigenfrequencies of assembly HT + cavity

n.	f [Hz]	Mode Shape
1	27.77	
2	51.66	
3	116.1	
4	305.9	

Acknowledgements

We acknowledge the support of the European Community-Research Infrastructure Activity under the FP6 “Structuring the European Research Area” programme (CARE, contract number RII3-CT-2003-506395)

References

- [1] M. Liepe, W.D.-Moeller, S.N. Simrock, “Dynamic Lorentz Force Compensation with a Fast Piezoelectric Tuner”, Proceedings of the 2001 Particle Accelerator Conference, Chicago, p. 1074-1076
- [2] H. Kaiser, “New Approaches to Tuning of TESLA Resonators”, in Proceedings of SRF Workshop 1999, Santa Fe, USA.
- [3] D. Barni, A. Bosotti, C. Pagani, R. Lange, H.B. Peters, “A new tuner for Tesla”, Proceedings of EPAC 2002, Paris, France, 2205-2207
- [4] TESLA Technical Design Report, DESY 2001-011, 2001
- [5] R. Mitchell, K. Matsumoto, G. Ciovati, K. Davis, K. Macha, R.Sundelin, “Lorentz force detuning analysis of the spallation neutron source (SNS) accelerating cavities”, 10th Workshop On RF Superconductivity (SRF 2001), Tsukuba (JP), 09/06/2001--09/11/2001.
- [6] P. Sekalski et al., “Static Absolute Force Measurement for Preloaded Piezoelements used for Fast Lorentz Force Detuning System”, in Proceedings of Linac 2004, Lubeck, Germany, p. 486.

Appendix 1: Summary of piezo properties

PROPERTIES	unit / tolerance	Noliac	PI
		SCMA/S1/A/10/10/40/200/60/4000	P-888.90
Room Temperature			
material		medium soft doped PZT-S1	PZT-PIC 255
case/preload		no	no
length	mm	40 ± 0.5	36
active length	mm	38.5	33.84
cross section	mm x mm	(10 x 10) ± 0.2	10 x 10
Number of layers		266	300
Average layer thickness	µm	140	113
Young modulus	kN/mm ²	45	48.3
stiffness	kN/µm	0.1125	0.105
max. stroke	µm	60 ± 9	35 ± 3.5
blocking force (closed loop)	N	4000 ± 800	3600 ± 720
max. load	N	12000	10000
Parallel Res. Frequency @ no load	kHz	38	40
density	kg/m ³	7.7 x 10 ³	7.8 x 10 ³
min. voltage		0	-20
max. voltage	V	200	120
control speed - unloaded	V/µs		
charge current	A		
capacity: nominal	µF	8	12.4
measured	µF	8.3	13.6
Loss Factor	tanδ	0.017	0.015
Thermal Expansion Coefficient (Multilayer)	Ppm/K	-2.5	
Cryogenic Measurements, T = 4.2 K			
Parallel Res. Frequency @ no load	kHz		48.5
Capacity @ no load	µF		5.7
Cryogenic Measurements, T = 2 K			
Parallel Res. Frequency @ no load	kHz		52.5
Capacity @ no load	µF		3.5
Expected Values			
Capacity @ T = 4.2 K	µF	3.4	
Capacity @ T = 2 K	µF	2.1	
Stroke @ T = 4.2 K	µm	6	7
Stroke @ T = 2 K	µm		
Parallel Res. Frequency @ no load, T = 4.2 K	kHz	46	
Parallel Res. Frequency @ no load, T = 2 K	kHz	50	

Appendix 2: Technical Drawings

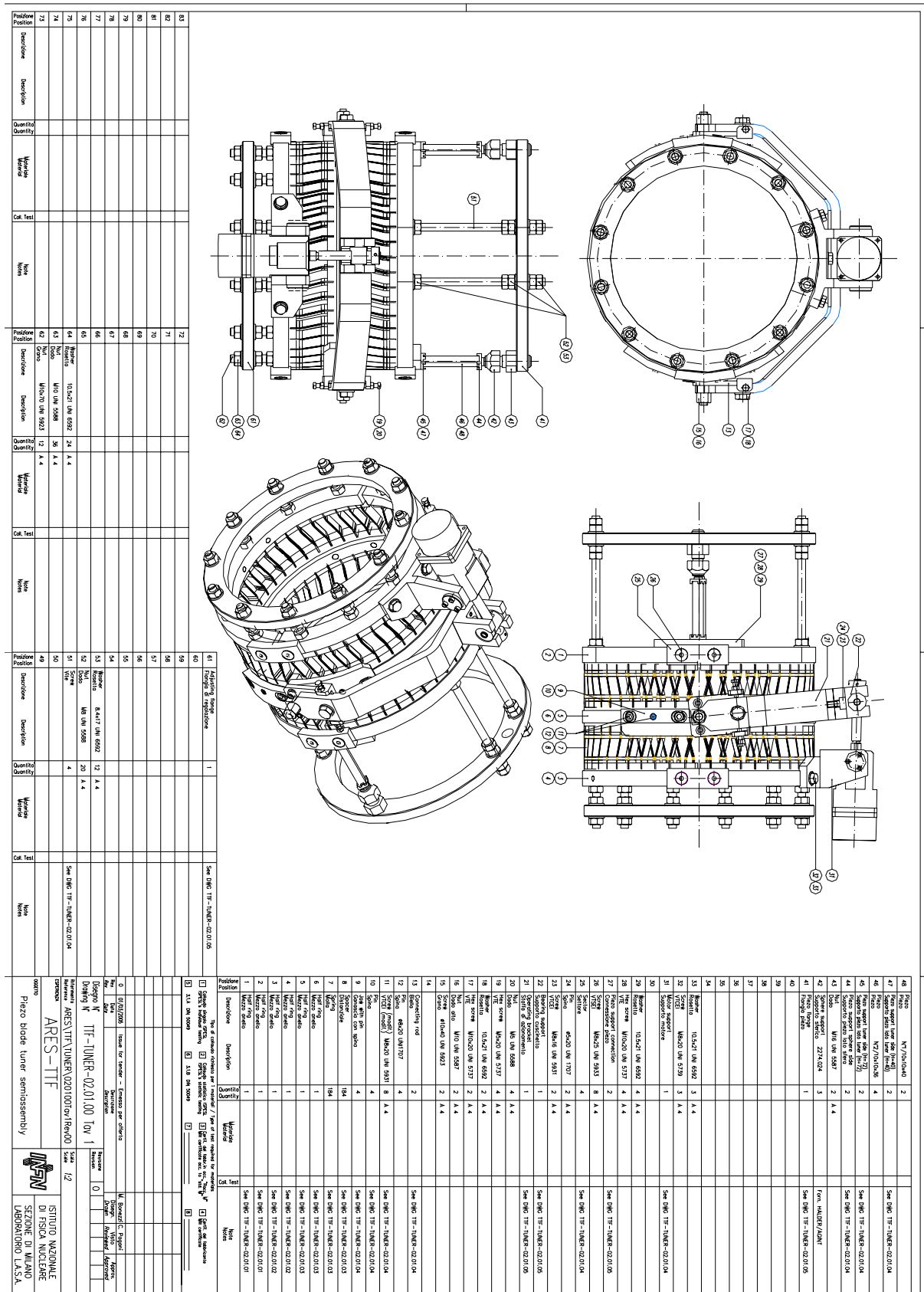


Figure 28: Piezo blade tuner technical drawings. The single tuning part and detail drawing numbers are here reported for reference.